Available online at www.sciencedirect.com
SCIENCE DIRECT
Cement and Concrete Research 36 (2006) 912 – 920
Cement and Concrete Research

Effect of applied stresses on alkali–silica reaction-induced expansions

Stéphane Multon [a,*], François Toutlemonde [b]

[a] Laboratoire Matériaux et Durabilité des Constructions INSA-UPS Complexe Scientifique de Rangueil 135, ave de Rangueil 31077 Toulouse Cedex 4, France
[b] Laboratoire Central des Ponts et Chaussées 58, bld Lefebvre 75732 Paris, Cedex 15, France

Received 10 October 2005; accepted 11 November 2005

Abstract

The mechanical effects of alkali–silica reaction (ASR) have to be modeled in order to assess the deterioration level and the stability of ASR-damaged concrete structures. Several experimental programs have shown the effects of compressive stresses on ASR-induced strains. The effect is so significant that assessment models have to take into account the modification of ASR expansions due to applied stresses and the consequences on the mechanical response of damaged structures. This paper presents and analyzes measurements performed on concrete specimens subjected to several states of stresses along the three directions (due to applied stresses and to passive restraint). Mechanical calculations show that the volumetric expansion imposed by ASR is constant whatever the stresses conditions. They point out the "expansion transfer" occurring along the directions which are less compressed; thus, the effect of stresses on ASR expansions anisotropy can be precisely quantified.

Keywords: Alkali–aggregate reaction (C); Anisotropy; Expansions (C); Modeling (E); Stress effect (C)

1. Introduction

Alkali–silica reaction (ASR) affects some significant bridges and civil engineering structures, and assessment methods are still required in order to answer the questions of the owners of ASR-damaged structures. Several researchers developed models and methods in order to evaluate the degradation of ASR-damaged structures [1–3]. However, the effect of one major parameter is still badly known: the effect of applied stresses on ASR-induced strains.

During all their service life, civil engineering structures may be subjected to large mechanical stresses. The consequences of such loading conditions on ASR-induced expansions had to be determined. Numerous experimental programs have shown that compressive stresses caused the decrease of ASR expansion along the compressed direction [4–7]. For this reason, ASR-induced strains are reduced by the reinforcing steels [8–12]. Therefore, assessment models have to take into consideration the property of stresses to modify ASR-induced expansions and their effect on the mechanical response of ASR-damaged structures like dams, which are highly stressed structures, and bridges, which are highly reinforced structures.

This paper presents and analyzes measurements carried out on concrete specimens subjected to several states of stresses along the three directions. These experiments were part of an important program co-sponsored by EDF, the French Power Company, and LCPC, the French Public Works Research Agency [13]. In the past, most papers have based their investigations on the measured strains. Such an analysis allows the ASR-consequences on structures to be assessed, but does not quantify the variation of ASR-induced expansions under 3D states of stresses. In the present study however, the numerous experimental data obtained on about fifty specimens have been analyzed using the basic assumption that ASR-induced strains can be represented as imposed strains [1,2]. The consequences of stresses on ASR-induced volumetric expansion and ASR anisotropic development are then emphasized and quantified, which can further be used in order to validate or improve ASR models.

2. Experimental data

The effects of applied stresses on ASR-induced expansion were extensively investigated on two concrete mixtures with a

* Corresponding author. Tel.: +33 5 61 55 67 11.
E-mail address: multon@insa-toulouse.fr (S. Multon).

0008-8846/$ - see front matter © 2005 Elsevier Ltd. All rights reserved.
doi:10.1016/j.cemconres.2005.11.012

Fig. 1. Creep devices (4 specimens by device).

0.5 water/cement ratio and a 410 kg/m^3 cement content: one "reactive" mixture with siliceous limestone aggregate containing reactive silica and one "reference" mixture with aggregate without reactive silica [13]. Potassium hydroxide was dissolved in the mixing water in order to increase the Na_2O_{eq} content (up to 1.25% of the mass of cement). Moisture content has large effects on ASR-expansions [14,15]. Therefore, all the specimens were kept sealed under a watertight cover in order to obtain a homogeneous moisture state and thus homogeneous ASR-induced strains in the whole specimens.

After 28 days of curing, nine different states of stresses were applied to cylindrical specimens (130 mm in diameter and 240 mm height) during 450 days. The axial stresses were applied by flat hydraulic jack within closed frames usually used as creep devices (Fig. 1) [15]. The radial stresses were resulting from lateral restraint provided by steel rings, 3- or 5-mm-thick (Fig. 2 – steel yield stress=206 MPa, Young's modulus=193,000 MPa). The contiguous 10-mm-high rings externally confined expansive concrete. They were not connected, so that longitudinal restraint due to these rings was eliminated. When

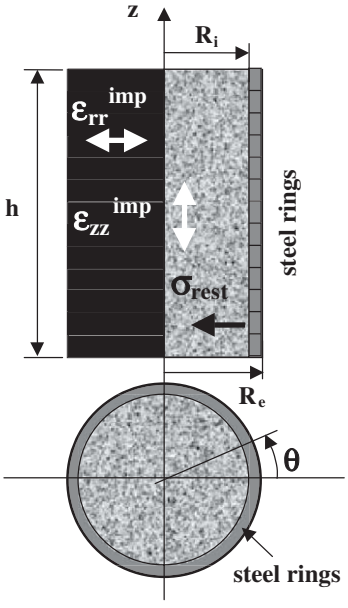

Fig. 2. Passive restraint by steel rings.

Table 1
Characteristics of the 48 specimens

		Restraint		
		None	3 mm	5 mm
Applied stresses	0 MPa	4R+4NR	4R	4R
	10 MPa	4R+4NR	4R	4R
	20 MPa	4R+4NR	4R	4R

R: reactive concrete, NR: non-reactive concrete.

the reactive concrete cast within the rings progressively tends to expand due to ASR, the radial and tangential stresses increase homogeneously within the concrete cylinder, depending on the rings thickness. Reactive concrete was submitted to all combinations of three axial stresses (0, 10 and 20 MPa) and three transverse restraint levels (none, 3-mm-thick rings, 5-mm-thick rings – Table 1). Reference concrete was only submitted to axial loading (due to insufficient lateral strains for inducing measurable restraint). Four specimens were tested for each condition.

Applied stresses and resulting strains were measured separately. Indeed, the strains of the specimens were monitored externally, using an automated device (Fig. 3) deriving from the one described by Larive et al. [4]. The mean transversal strain is based on diameter variations measured at 3 levels of the cylinders, at 10 regularly spaced angular locations. For this experiment, the target of the sensors was directly the outer surface of the specimens – either steel rings, or concrete. Absolute uncertainty is about 0.002% (i.e. 20 μm/m). The mean longitudinal deformation derives from 14 length variations regularly spaced around the cylinder. It is measured between two metallic targets glued to the ends of the specimens on a 0.240 m basis. For this direction, the boundary settlements were thus included in the measure. Strains were monitored every two weeks, until stabilization at about 450 days.

3. Theoretical analysis

3.1. Chemo-mechanical modeling

Assuming that ASR-induced strains can be considered as imposed strains [1,2], the aim of the following analysis is to

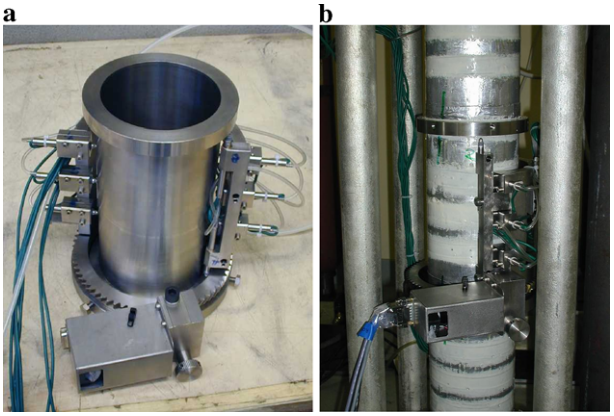

Fig. 3. Strain measurements of specimens by an automated device: (a) steel reference cylinder; (b) in operation on an axially loaded specimens.

identify these imposed strains, which are postulated to be assumed in order to obtain the deformations measured on the specimens. Since stresses in concrete along the three directions can be calculated, the imposed strains in the three directions can be related to the stress state. ASR-induced strains ("chemical"-imposed strains) read:

$$\underline{\underline{\varepsilon_{imp}}} = \begin{pmatrix} \varepsilon_{imp}^{rr} & 0 & 0 \\ 0 & \varepsilon_{imp}^{\theta\theta} & 0 \\ 0 & 0 & \varepsilon_{imp}^{zz} \end{pmatrix} \quad (1)$$

It has already been shown that ASR-induced strains are highly anisotropic compared to casting direction [16–19]: the ASR-induced expansions along the casting direction are larger than the expansions measured along the two other directions. For these cylindrical specimens, the casting direction is vertical, consistently with the cylindrical symmetry of specimens, the chemical expansions can thus be assumed as orthotropic: $\varepsilon_{imp}^{\theta\theta}=\varepsilon_{imp}^{rr}$. In addition, for these sealed specimens, the water content (which highly influences ASR-expansions) can be assumed as roughly constant during the whole study and equal for all specimens. Therefore, the ASR-imposed strains can be assumed, in a first approach, as homogeneous in the whole specimens.

The concrete constitutive law is assumed as chemo-elastic and takes into account the chemical expansions due to ASR [1,2], which reads:

$$\underline{\underline{\sigma}} = \left(K_c - \frac{2}{3}G_c\right) tr\,\underline{\underline{\varepsilon}}\;\underline{\underline{I}} + 2G_c\,\underline{\underline{\varepsilon}} - 3K_c\,\underline{\underline{\varepsilon_{imp}^{(t)}}} \quad (2)$$

while the steel constitutive law only considers the elastic effect of steel rings:

$$\underline{\underline{\sigma}} = \left(K_s - \frac{2}{3}G_s\right) tr\,\underline{\underline{\varepsilon}}\;\underline{\underline{I}} + 2G_s\,\underline{\underline{\varepsilon}} \quad (3)$$

where K and G read for each material:

$$K = \frac{E}{3(1-2\nu)} \quad (4)$$

and

$$G = \frac{E}{2(1+\nu)} \quad (5)$$

where E is the Young's modulus and ν is the Poisson's coefficient.

The stresses in the two materials have to verify the equilibrium equation: $\underline{\mathrm{div}}\,\underline{\underline{\sigma}} = 0$ in the cylindrical basis ($\underline{e_r}$, $\underline{e_\theta}$, $\underline{e_z}$). The resolution of the equilibrium equation and the symmetries of the mechanical problem allow the displacements in the two materials to be written:

In concrete:

$$\underline{u^c}(r;z) = Ar\,\underline{e_r} + Bz\,\underline{e_z} \quad (6)$$

In the vertically disconnected steel rings:

$$\underline{u^s}(r) = \left(Cr + \frac{D}{r}\right)\underline{e_r} \quad (7)$$

Strains can then be derived:

In concrete:

$$\varepsilon_{rr}^c = \frac{\partial u_r^c}{\partial r} = A \text{ and } \varepsilon_{\theta\theta}^c = \frac{u_r^c}{r} = A \text{ and } \varepsilon_{zz}^c = \frac{\partial u_z^c}{\partial z} = B \quad (8,9,10)$$

In the steel rings:

$$\varepsilon_{rr}^s = \frac{\partial u_r^s}{\partial r} = C - \frac{D}{r^2} \quad (11)$$

$$\varepsilon_{\theta\theta}^s = C + \frac{D}{r^2} \quad (12)$$

and

$$\varepsilon_{zz}^s = 0 \quad (13)$$

Four unknown constants (A, B, C, D) have been introduced. They have to be determined from the boundary conditions:

– The axial stresses at the ends of the specimens are equal to externally applied stresses:

$$\sigma_{zz}^c(h) = \sigma_{zz}^c(0) = \sigma_{zz}^{appl} \quad (14)$$

– The radial displacements at the interface between steel and concrete are equal:

$$u_r^s(R_i) = u_r^c(R_i) \quad (15)$$

– The radial stress on the external surface is equal to zero:

$$\sigma_{rr}^s(R_e) = 0 \quad (16)$$

– The radial stresses in concrete and in steel at the interface are equal.

$$\sigma_{rr}^s(R_i) = \sigma_{rr}^c(R_i) = \sigma_{rest} \quad (17)$$

Moreover, it derives from Eqs. (2), (6) and (8–10) that radial and tangential stresses are constant in the whole concrete and equal to σ_{rest}, the "stress due to restraint".

Imposed strains shall be identified from the deformations measured on specimens. These measured data allow two supplementary equations to be written. The axial stress was only applied on the concrete and the deformations measured axially by the automated device can be directly identified as the axial deformations of concrete:

$$\varepsilon_{zz}^c = \varepsilon_{zz}^{meas} = \frac{u_{zz}^{meas}}{h} = \frac{\partial u_z^c}{\partial z} = B \quad (18)$$

In the case of the specimens confined by steel rings, the measured radial displacements can not be related directly to material deformations. However, they lead to a displacement determination at the external surface:

$$u_r^s(R_e) = CR_e + \frac{D}{R_e} = u_r^{meas} \quad (19)$$

The six equations (Eqs. (14) (15) (16) (17), (18) and (19)) allow the mechanical problem to be solved. The stress due to the restraint of steel rings can be derived from the radial displacement measured on the specimens:

$$\sigma_{rr}^s(R_i) = \sigma_{rest} = 2G_s\left(\frac{K_s + \frac{1}{3}G_s}{K_s + \frac{4}{3}G_s}\right)\left(\frac{1}{R_e} - \frac{R_e}{R_i^2}\right)u_r^{meas} \quad (20)$$

Following expressions can be derived in order to identify the ASR-induced strains from measured deformations:

$$\varepsilon_{rr}^{imp} = -\frac{1}{3K_c}\left(\sigma_{rest} - \left(2K_c + \frac{2}{3}G_c\right)A - \left(K_c - \frac{2}{3}G_c\right)B\right) \quad (21)$$

$$\varepsilon_{zz}^{imp} = -\frac{1}{3K_c}\left(\sigma_{zz}^{appl} - \left(K_c - \frac{2}{3}G_c\right)2A - \left(K_c + \frac{4}{3}G_c\right)B\right) \quad (22)$$

where

$$A = \frac{u_r^{meas}G_s}{R_e\left(K_s + \frac{4}{3}G_s\right)}\left[1 + \left(\frac{1}{3} + \frac{K_s}{G_s}\right)\frac{R_e^2}{R_i^2}\right] \quad (23)$$

and B is given by Eq. (18).

Thus, the imposed strains can be written:

$$\begin{cases}\varepsilon_{rr}^{imp} = E_1 u_r^{meas} + E_2\varepsilon_{zz}^{meas} \\ \varepsilon_{zz}^{imp} = -\dfrac{\sigma_{zz}^{appl}}{3K_c} + E_3 u_r^{meas} + E_4\varepsilon_{zz}^{meas}\end{cases} \quad (24)$$

where E_1, E_2, E_3 and E_4 are coefficients which only depend on material mechanical properties and on specimens dimensions. Moreover, $R_e = R_i$ corresponds to the case of specimens free of restraint.

3.2. Application to data processing

Measured data were obtained directly from average differences in LVDT sensors output of the automated device. The deformations measured at the moment of load application were affected by the boundary settlements, which caused apparent strains larger than those caused by the only behavior of concrete. Therefore, all the measured data presented in this paper take into account an offset just after the initial mechanical loading.

For the specimens with steel rings, an apparent radial deformation can be defined by the ratio of the radial displacement measured on the steel rings to the radius of specimen. It does not really correspond to deformations of one material, but it allows the behavior of all the specimens to be compared. Thus, the effect of steel rings on the measured strains can be analyzed [7].

The measurements were performed on four specimens for each stress state. In the whole paper, the measured data are represented by the mean value and the standard deviation of the four measurements. The standard deviation quantifies the ASR expansion heterogeneity, which can be explained by the heterogeneous repartition of the reactive silica inside the limestone aggregate [17] and by the heterogeneous repartition of reactive aggregate in specimens. All the causes of uncertainty on these measurements (uncertainty on strain measurements, mechanical properties, etc.) can be neglected compared to the intrinsic ASR-scatter.

The stresses due to the restraint of steel rings have been calculated from Eq. (20). For this calculation, the total strains (including shrinkage, creep and ASR-induced expansions) affect the restraint and were taken into account.

On the contrary, ASR-imposed strains have to be identified from the deformations measured on specimens, without taking into consideration the other mechanisms. During the experiment, the deformations were measured on reference sealed specimens which were subjected to shrinkage and/or to basic creep (as shown in Figs. 4 and 5). On the free-expanding reference specimens, large shrinkage strains were observed during the first 60 days, before stabilization (Figs. 4 and 5). It was due to autogeneous shrinkage and to residual drying shrinkage caused by tightness defects of the specimens cover (mass losses of less than 0.5% after 450 days were measured). Shrinkage strains after 100 days were quite constant, which illustrates that the effect of drying through the sealing was quite small. In order to take into account the only effect of ASR expansions, the shrinkage and the creep strains measured on the reference specimens have been withdrawn from the deformations measured on the reactive specimens. The ASR-imposed strains can be deduced from the Eq. (24), leading to:

$$\begin{cases}\varepsilon_{rr}^{ch} = E_1\left(u_{r/Reac}^{meas} - u_{r/Ref}^{meas}\right) + E_2\left(\varepsilon_{zz/Reac}^{meas} - \varepsilon_{zz/Ref}^{meas}\right) \\ \varepsilon_{zz}^{ch} = E_3\left(u_{r/Reac}^{meas} - u_{r/Ref}^{meas}\right) + E_4\left(\varepsilon_{zz/Reac}^{meas} - \varepsilon_{zz/Ref}^{meas}\right)\end{cases} \quad (25)$$

The effect of ASR-heterogeneity on the scatters of calculations has been assessed by calculating the standard deviation of calculated values resulting from the standard deviation of measurements.

The elastic calculations have been performed with the following mechanical properties: 193,000 MPa and 0.3 for the steel Young's modulus and Poisson's ratio. For the reactive concrete, Poisson's ratio was measured at several time-steps. The Poisson's ratio was constant and equal to 0.22 [13,19]. The evolutions of instantaneous Young's modulus of ASR-affected concrete are still discussed [8,12,15,18]. For this concrete mixture, the evolution appears to be quite small [13,19]. Therefore, it has been taken equal to its initial value (37,300 MPa) for all these first approach calculations.

In fact, the shrinkage and the longitudinal creep have been taken into account for all specimens by withdrawing longitu-

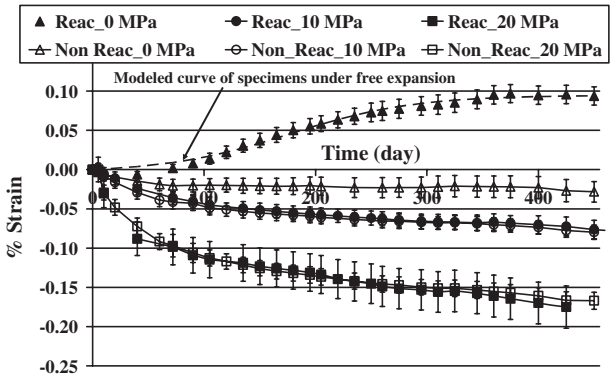

Fig. 4. Measured axial strains of the reactive and reference specimens under axial loading only (for specimens under free expansion, Larive's model led to: latency time: 177 days, characteristic time: 55 days, and asymptotic strain: 0.095%).

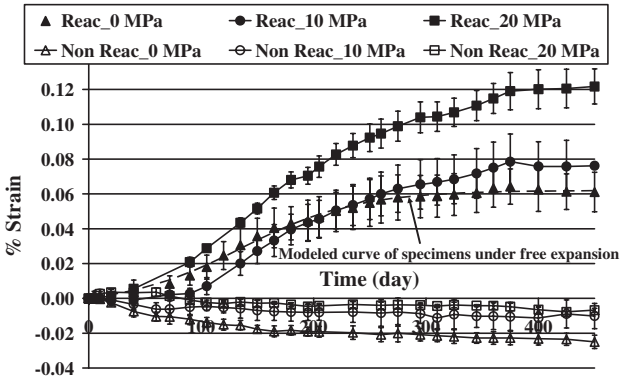

Fig. 5. Measured radial strains of the reactive and reference specimens under axial loading only (for specimens under free expansion, Larive's model led to: latency time: 135 days, characteristic time: 52 days, and asymptotic strain: 0.062%).

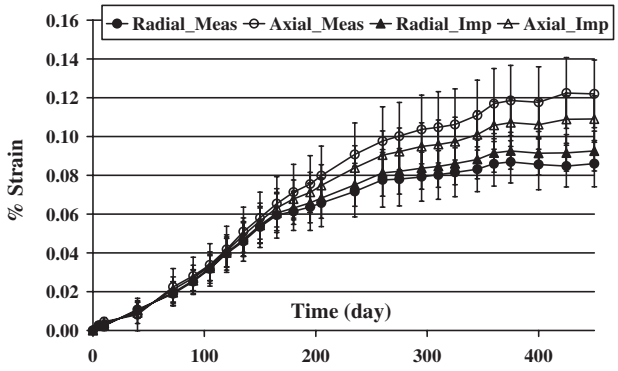

Fig. 6. Specimens under "free expansion" – Radial and axial «measured» strains (in fact, the difference between the strains measured on the reactive specimens and the strains measured on the reference ones) and chemical imposed strains.

dinal strains of reference specimens. However, the compressive stress due to the restraint of steel rings also causes lateral creep, which can not be assessed with the reference specimens. In order to take into consideration this creep, the concrete Young's modulus (which acts on E_1 and E_2 values) has been taken equal to long term Young's modulus. It has been evaluated by considering the instantaneous and delayed strains of the reference concrete. It can not be directly determined by the deformations measured on reference specimens due to boundary settlements. However, the reference instantaneous Young's modulus was measured on reference specimens 28 days after casting (37,200 MPa). Thus, instantaneous strains of reference concrete can be assessed to 0.027% and 0.054% under 10 MPa and 20 MPa. Moreover, the delayed strains were about 0.080% and 0.167% after 400 days under 10 MPa and 20 MPa (Figs. 4 and 5), leading to a ratio of about 3 between delayed and instantaneous strains. Therefore the long term Young's modulus has been obtained by dividing the instantaneous Young's modulus by 4.

4. Analysis of the experimental results

4.1. Free ASR expansion test

The measurements carried out on the specimens under free expansion exhibit the classical time-evolution of ASR-induced strains which can be described by Larive's model [1,15]: latency times of about 135 and 177 days, characteristic times of about 52 and 55 days and asymptotic strains of about 0.062% and 0.095% for the radial and the axial directions, respectively (Figs. 4 and 5).

Data measured both on reactive and reference specimens without externally applied load have been used as input data in the systems of Eq. (25); the results of calculations have been plotted in Fig. 6. It is important to note that the obtained "imposed" strains differ from the "measured" strains. This difference can be explained by the Poisson's effect. In fact, imposed strains along one direction act on the measured strains along perpendicular directions. This constitutes a major difference between this analysis based on ASR-induced strains, as compared to direct analysis of measurements [7,15].

The observed difference between measured radial and axial strains, thus tends to overestimate the anisotropy coefficient, considered as the ratio between the axial and the radial-imposed strains. Anisotropy of ASR-imposed strains appears to be constant during free expansion tests without externally applied load (Fig. 7). Anisotropy was about 1.15 which is quite close to unity, and far from previously reported values (about 2 in [13,15,17,19]). The anisotropy of ASR-expansions during free expansion tests is a complex phenomenon. Several papers noted that the ASR-expansions are always larger perpendicular to cracks; and concluded that anisotropy was influenced by the directions of the cracks [15–17]. In previous study, the anisotropy value was determined on specimens kept in wet environment [15,17]. ASR-expansions measured in such conditions were larger than ASR-expansions measured on sealed specimens as presented in this paper. Larger ASR-expansions caused more cracks and can cause a larger ASR-anisotropy. In the papers [13,19], ASR-anisotropy equal to 2 was determined on sealed specimens. The radial and axial expansions were measured on different specimens. Mass losses were observed and evaporation through watertight cover can be suspected [13,19]. Such evaporation caused heterogeneity in the conditions of the specimens and can explain a larger value of anisotropy than for the present study.

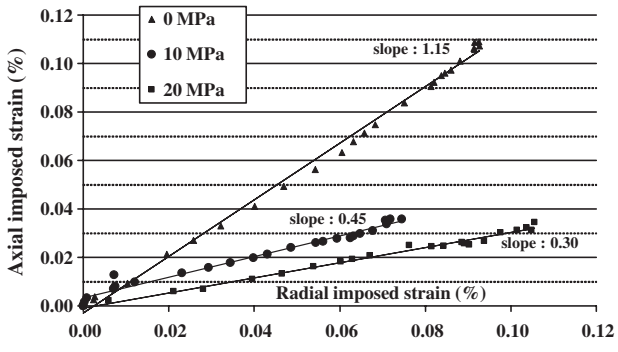

Fig. 7. Axial imposed strains versus radial imposed strains for the reactive specimens without restraint.

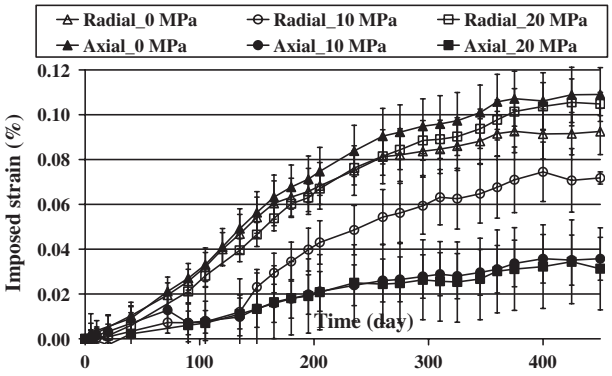

Fig. 8. Axial and radial imposed strains for reactive specimens, under axial loading only.

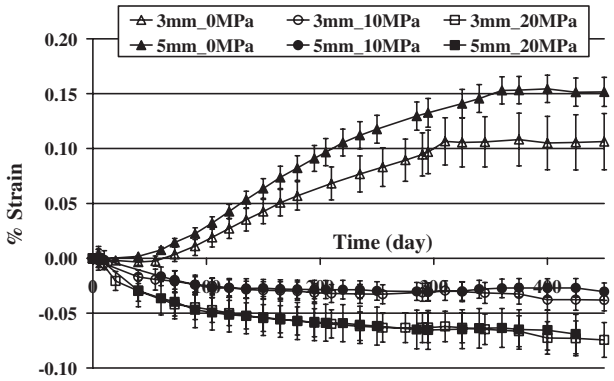

Fig. 9. Axial measured strains for the reactive specimens with 3 mm and 5 mm restraints under varied axial loads.

4.2. Specimens under longitudinal applied loading only

The strains measured on reactive specimens under longitudinal applied loading have been compared to measurements on reference concrete and to reactive specimens under free expansion (Figs. 4 and 5). The creep axial behavior of both types of concrete is quite similar for both levels of applied loading with delayed axial strains of about 0.075% and 0.170% under 10 MPa and 20 MPa (Fig. 4). The reactive specimens exhibit significant radial expansions: the larger the axial load, the larger the expansions (0.08% and 0.12% under 10 and 20 MPa compared to 0.06% for the specimens under free expansion). The non reactive specimens show negative radial strains (about 0.01% and 0.02%) due to shrinkage.

Axial ASR-imposed strains are plotted in Fig. 8 for reactive specimens submitted to axial loading only. Classical analysis based on measurements on specimens under applied load show that the strains measured along compressed directions are completely null for applied loads higher than 5 MPa [7,15]. However, imposed axial strains are not null. In fact, due to the axial load, asymptotic ASR-imposed expansions are only partly reduced, from about 0.1% to 0.03%, whatever the 10 or 20 MPa applied stress level. Radial ASR-imposed strains slightly increase, it may be explained by an "expansion transfer": when a high enough external compression is applied, ASR gel products preferably expand in transverse – less compressed – directions.

Axial versus radial-imposed strains have been plotted in Fig. 7; a constant slope of the experimental plots is obtained, known as "anisotropy coefficient". The ASR anisotropy coefficient is about 0.45 for reactive specimens under 10 MPa and 0.30 for specimens under 20 MPa (Fig. 7). This coefficient gives a precise and meaningful description of the mechanism of "expansions transfer" due to compressive stresses and presented in [4].

4.3. Confined specimens

For the measured longitudinal strains on specimens under restraint, three groups of curves can be distinguished according to the axial load (Fig. 9). Specimens without axial applied load show axial ASR expansions (between 0.10% and 0.15% for specimens confined with 3 mm and 5 mm rings), while for loaded specimens, the negative deformations show that the creep strains were larger than ASR expansions, with a negligible effect of the rings thickness (Fig. 9). The negative strains reach only 0.030% for 10 MPa and 0.075% for 20 MPa, compared to 0.075% and 0.170% for the same loading on the unrestrained specimens (Fig. 4). Therefore, the rings have a real effect on the axial strains. Radial measured strains are lower and more disturbed by the heterogeneity and scatter of expansions measurements (Fig. 10). The larger scatter of these results (±500 μm/m) appears as specific to the radial measurements of specimens under restraint (and particularly with 5-mm-thick rings) and can be explained by some metrological problems when the target of the sensors is located at the limit of the steel rings [13].

Compressive stresses were caused along the radial direction by the passive restraint of steel rings. The compressive stresses can be assessed by Eq. (20) for all confined specimens (Fig. 11). It gives consistent results: for the same applied load, the thicker the steel rings, the larger the restraint stress. The restraint stresses along the radial direction lie between 1 MPa and 12.5 MPa. For the specimens without axial loading, the radial stresses in concrete due to restraint are really low (between 1 and 3 MPa); most of ASR-expansions occurred along the axial direction free of restraint. For the specimens with axial loading, the radial stresses are always lower than the

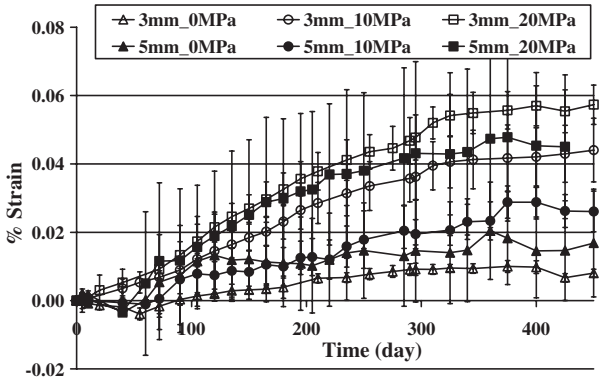

Fig. 10. Radial measured strains for the reactive specimens with 3 mm and 5 mm restraints under varied axial loads.

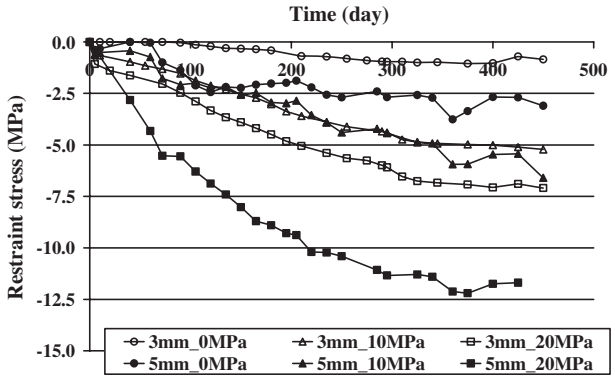

Fig. 11. Radial compressive stresses due to passive restraint of ASR induced expansions.

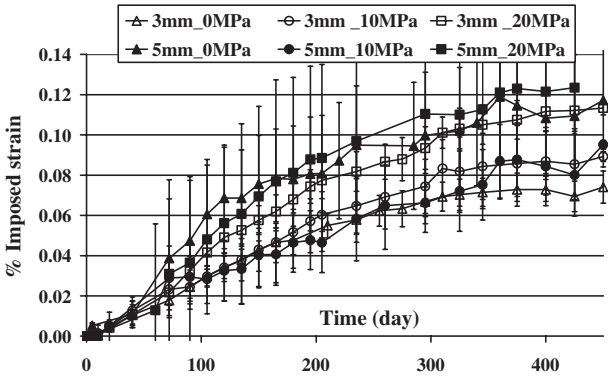

Fig. 13. Radial imposed strains for reactive specimens with 3 mm and 5 mm restraints under varied axial loads.

axial stresses (between 5.5 and 6.5 MPa vs. 10 MPa and between 7.5 and 12.5 MPa vs. 20 MPa); the axial direction is the most compressed direction. Calculations show that the higher the axial stress is, the larger the radial stress would be. This result can be explained by larger ASR-induced expansions along the less compressed direction, which is consistent with "ASR-expansion transfer" concept.

ASR-imposed strains have been identified for the specimens under lateral restraint and possible axial loads, and are plotted in Fig. 12 (axial-imposed strains) and Fig. 13 (radial-imposed strains). The axial-imposed strains are larger for the unloaded specimens (0.10% and 0.13% for the 3-mm and 5-mm steel rings) than for loaded ones (lower than 0.08% for all the confined specimens). Moreover, for the unloaded specimens, the thicker the steel rings, the greater the longitudinal imposed strains (0.10% for the 3 mm rings compared to 0.13% for the 5 mm ones), in spite of low radial stresses (between 1 and 3 MPa). Results may appear as more confused along the radial direction and particularly for 5-mm-thick restraint (Fig. 13). However, for the 3-mm-thick steel rings, the lower the axial stress, the lower the radial ASR-imposed strains (0.115%, 0.09% and 0.075% for 20, 10 and 0 MPa) All these previous observations illustrate the "expansion transfer". The radial-imposed strains appear to be more dependent on the axial load than on the rings thickness. Indeed, the values of the radial-imposed strains for the two applied axial loads are close, whatever the rings thickness (0.09% and about 0.12% for 10 and 20 MPa – Fig. 13). They are even close to results of the loaded specimens free of restraint (0.07% for 10 MPa and 0.11% for 20 MPa – Fig. 8). Since the compressive restraint stress always stayed lower than axial stresses when an axial load was applied, the "expansion transfer" occurred along the radial direction, which is the less compressed direction.

Finally, the best quantification of "expansion transfer" appears to be the ASR anisotropy coefficient. Indeed, this coefficient is constant during the whole study period for all the specimens while all the other values, and particularly the chemical-imposed strains, change. Moreover, it perfectly characterizes the ratio of imposed strains between the three main directions of the mechanical problem. The calculations have been carried out for all the specimens (Figs. 14 and 15). Since scatter around axial and radial ASR-induced imposed strains results in variations of about 0.20 around the coefficient of anisotropy, the values are presented with a 0.05 resolution. The anisotropy coefficient for the unloaded specimens restrained by 3 mm thick rings is 1.40 compared to 1.15 for specimens under free expansion. For specimens with 5 mm restraint and no axial load, Fig. 14 shows clearly that two slopes can be calculated: the first is about 0.75 and the second one about 1.65. These measurements are especially disturbed during the first 100 days (Fig. 10) due to metrological problems described above. Thus, the second slope is considered as more reliable. For all the specimens under 3D states of stresses, the anisotropy coefficients lie between 0.4 and 0.5. It shows that the ASR-imposed strains are mainly reduced along the axial

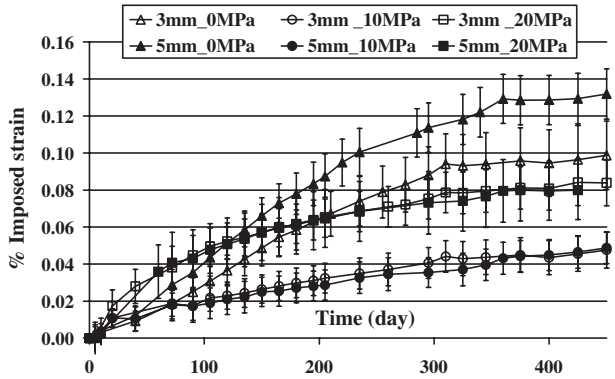

Fig. 12. Axial imposed strains for reactive specimens with 3 mm and 5 mm restraints under varied axial loads.

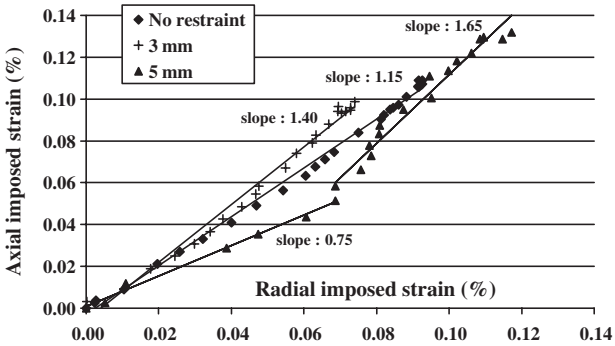

Fig. 14. Axial imposed strains versus radial imposed strains for reactive specimens without axial applied load.

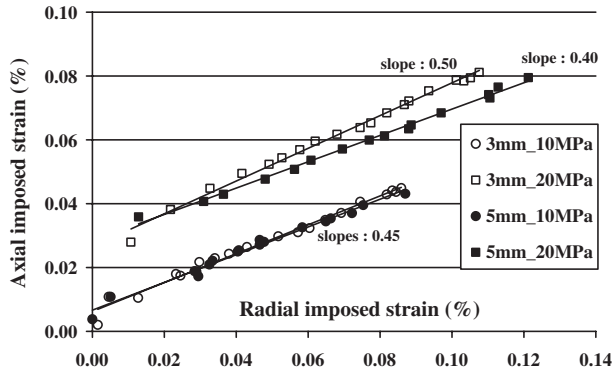

Fig. 15. Axial imposed strains versus radial imposed strains for reactive specimens with combined axial load/lateral restraint.

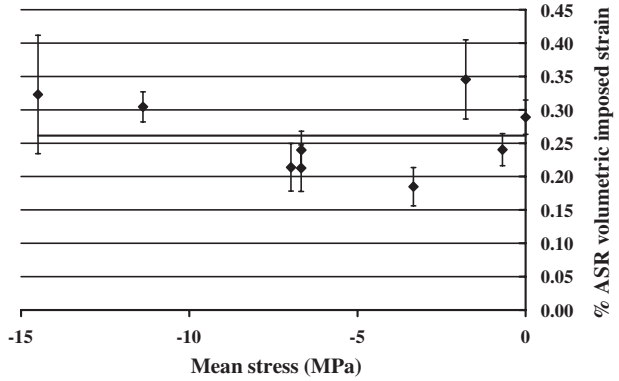

Fig. 17. Volumetric asymptotic imposed strain versus mean stress at 400 days.

direction. This result appears to be consistent with a previous note: as long as the compressive restraint stress stays lower than the axial stress, the "expansion transfer" takes place along the less compressed direction.

5. Synthesis

The "expansion transfer" concept was first observed on specimens with one free direction [4]. During this previous experimental study, the classical analysis on measurements has been performed: the measured volumetric expansions appeared to be equal for both stress-free and axially loaded specimens while directional expansions depended on compressive stresses. For ASR-damaged specimens under 3D states of stresses, the measured volumetric expansions are reduced [7], but the classical analysis can not point out conclusions about real ASR-induced strains. Calculations carried out in this paper assess the real ASR-imposed strains. These ASR-induced deformations are more representative of the expansions imposed to damaged structures by ASR and allow the volumetric expansions to be calculated for the nine different states of stresses (1D and/or 3D). For such cylinders, the volumetric imposed strains are the sum of the axial ASR-imposed strain plus twice the radial-imposed strain. Taking into consideration the scatter of the results, Fig. 16 shows that the ASR volumetric imposed strains are quite close for all the states of stresses. In order to complete the analysis according to the state of stress, the ASR volumetric imposed strains have been calculated at the 400th day, when ASR deformations were stabilized and plotted at this time-step versus the mean stress. Fig. 17 shows that the ASR volumetric imposed strains lie between 0.18% and 0.35%, with a mean value of about 0.26% and a standard deviation of about 0.05% for all the nine states of stress. In comparison, the scatter of calculated volumetric imposed strains of each state of stress lies between 0.02% and 0.09% due to natural ASR heterogeneity, with a mean value of about 0.04%. Moreover, no trend can be noted between the ASR volumetric imposed strains and the stress state. Therefore, no difference can be statically proved and ASR volumetric imposed strains appear to be of the same order whatever the state of stress of concrete. The differences may be mainly due to ASR heterogeneity (and metrological problems).

At last, the "expansion transfer" concept is illustrated in Fig. 18, which represents the ASR anisotropy coefficient versus the axial stress deviator $D_{zz}=\sigma_{zz}-\sigma_{mean}$ (σ_{zz} is the axial stress and σ_{mean} is the mean stress).

– For negative axial stress deviator, the axial direction is more compressed than the radial one. In comparison with the free expansion test, compression reduces axial ASR-imposed strains, and, due to "expansion transfer" the radial ones are increased. Thus, the anisotropy coefficient decreases with the decrease of the axial stress deviator (with a minimum of about 0.30).

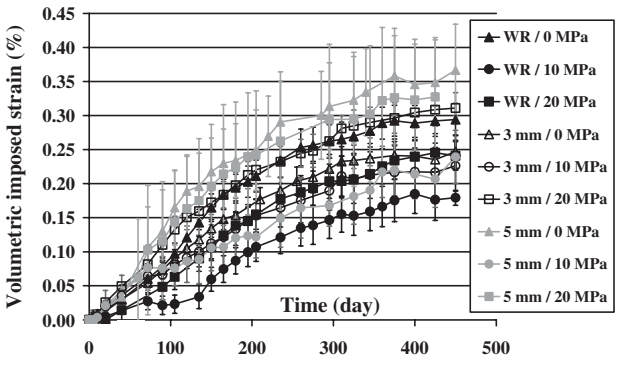

Fig. 16. ASR volumetric imposed strains for the nine states of stresses (WR: without restraint).

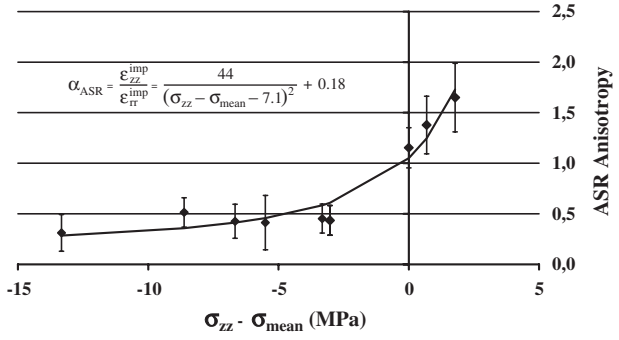

Fig. 18. "Expansion transfer": ASR anisotropy versus axial stress deviator.

– For positive stress deviator, the most compressed direction is the radial one and the anisotropy coefficient increases with the increase of the axial stress deviator.

The transfer has been observed as effective and can be important even for low stress deviator (slightly higher than 2 MPa). Such an evolution can be described by the following mathematical representation, obtained by best quadratic fitting of the results:

$$\text{For} \quad D_{zz} \leq 4 \text{ MPa} \quad \alpha_{ASR} = \frac{\varepsilon_{zz}^{imp}}{\varepsilon_{rr}^{imp}} = \frac{44}{(\sigma_{zz} - \sigma_{mean} - 7.1)^2} + 0.18 \tag{26}$$

The mean quadratic deviation between this mathematical representation and the anisotropy calculated from measurements is about 0.30, which is quite close to the scatter on the calculations of anisotropy coefficient (0.20). The asymptotic value for negative stress deviator (about 0.20) agrees with the observations made on the results of calculated ASR-imposed strains. For positive stress deviator, anisotropy coefficients cannot be infinite; they have to be limited to the inverse of the asymptotic coefficient obtained for negative stress deviator (about 5). Therefore, the anisotropy coefficient has to be fixed to a maximum value of 5 for stress deviator higher than 4 MPa (for higher stresses macroscopic cracking probably modifies the frame of hypotheses). As shown in Fig. 18, this mathematical representation of "expansion transfer" appears very satisfactory.

6. Conclusion

The aim of this paper was to analyze measurements on loaded and restrained specimens subjected to alkali–silica reaction, in order to discuss the need of structural models to account for the "expansion transfer" concept [4,7]. The following conclusions can be pointed out:

– Present investigations have validated the consistency of the approach which represents the ASR-induced expansions as isotropic imposed strains [1,2].
– Careful analyzing of the "stress-free" expansion test is mandatory, in order to take into consideration the Poisson's effect on 3D free expansion.
– The ASR volumetric imposed strain can be considered as constant whatever the stress state.
– In loaded and/or restrained concrete, ASR-induced expansions are transferred in the less compressed direction.

In order to carry out precise calculations to reassess ASR damaged structures, the structural models have to take into consideration this "expansion transfer" concept due to applied stresses. For models based on the assumption that ASR-induced strains can be represented by imposed strains, it can be obtained using the volumetric imposed strains as the basic input data, while the effect of anisotropy is deduced from the calculations of the stress deviator (using Eq. (26)).

Acknowledgements

The authors are pleased to thank LCPC technicians who participated in this research, and especially G. Leclainche who performed all the measurements presented in this paper. They acknowledge J-F. Seignol (LCPC) for his help in first calculations. They thank EDF for its support, and especially E. Bourdarot (EDF) and C. Larive (CETU, Lyon, France) for their effort in initiating this research.

References

[1] F.-J. Ulm, O. Coussy, K. Li, C. Larive, Thermo-chemo-mechanics of ASR expansion in concrete structures, J. Eng. Mech. 126 (3) (2000) 233–242.
[2] K. Li, O. Coussy, Concrete ASR degradation: from material modeling to structure assessment, Concr. Sci. Eng. 4 (2002) 35–46.
[3] B. Capra, A. Sellier, Orthotropic modelling of alkali–aggregate reaction in concrete structures: numerical simulations, Mech. Mater. 35 (2003) 817–830.
[4] C. Larive, A. Laplaud, M. Joly, Behavior of AAR-affected concrete: experimental data, Proc. 10th Int. Conf. AAR, Melbourne, Australia, 1996, pp. 670–677.
[5] T. Ahmed, E. Burley, S. Rigden, The effect of alkali–silica reaction on the fatigue behaviour of plain concrete tested in compression, indirect tension and flexure, Mag. Concr. Res. 51 (6) (1999) 375–390.
[6] C. Gravel, G. Ballivy, K. Khayat, M. Quirion, M. Lachemi, Expansion of AAR concrete under triaxial stresses : simulation with instrumented concrete block, Proc. 11th Int. Conf. AAR, Quebec, Canada, 2000, pp. 949–958.
[7] S. Multon, G. Leclainche, E. Bourdarot, F. Toutlemonde, Alkali–silica reaction in specimens under multi-axial mechanical stresses, Proc. 4th Int. Conf. CONSEC'04, Seoul, Korea, 2004, pp. 2004–2011.
[8] S. Inoue, M. Fujii, K. Kobayashi, K. Nakano, Structural behaviors of reinforced concrete beams affected by alkali–silica reaction, Proc. 8th Int. Conf. AAR, Kyoto, Japan, 1989, pp. 727–732.
[9] R.N. Swamy, M.M. Al-Asali, Control of alkali–silica reaction in reinforced concrete beams, ACI Mater. J. 87 (1990) 38–46.
[10] A.E. Jones, L.A. Clark, The effects of restraint on ASR expansion of reinforced concrete, Mag. Concr. Res. 48 (174) (1996) 1–13.
[11] S. Fan, J.M. Hanson, Length expansion and cracking of plain and reinforced concrete prisms due to alkali–silica reaction, ACI Struct. J. 95 (4) (1998) 480–487.
[12] T.U. Mohammed, H. Hamada, T. Yamaji, Alkali–silica reaction-induced strains over concrete surface and steel bars in concrete, ACI Mater. J. 100 (2003) 133–142.
[13] S. Multon, Evaluation expérimentale et théorique des effets de l'alcali-réaction sur des structures modèles, PhD thesis, Univ. Marne la Vallée, France, 2003 (in French).
[14] H. Olafsson, The effect of relative humidity and temperature on alkali expansion of mortar bars, Proc. 7th Int. Conf. AAR, Ottawa, Canada, 1986, pp. 461–465.
[15] C. Larive, Apports combinés de l'expérimentation et de la modélisation à la compréhension de l'alcali-réaction et de ses effets mécaniques, OA 28, ERLPC Collection, LCPC, Paris, 1998 (in French).
[16] L.A. Clark, Modeling the structural effects of alkali–aggregate reaction on reinforced concrete, ACI Mater. J. 88 (1991) 271–277.
[17] C. Larive, M. Joly, O. Coussy, Heterogeneity and anisotropy in ASR-affected concrete – consequences for structural assessment, Proc. 11th Int. Conf. AAR, Quebec, Canada, 2000, pp. 969–978.
[18] N. Smaoui, Contribution à l'évaluation du comportement structural des ouvrages d'art affectés de réaction alcali–silice (RAS), PhD thesis, Faculté des Sciences et de Génie de l'Université de Laval, Québec, Canada, 2003 (in French).
[19] S. Multon, J-F. Seignol, F. Toutlemonde, Structural behavior of concrete beams affected by alkali–silica reaction, ACI Mater. J. 102 (2) (2005) 67–76.